CERN – EUROPEAN ORGANIZATION FOR NUCLEAR RESEARCH

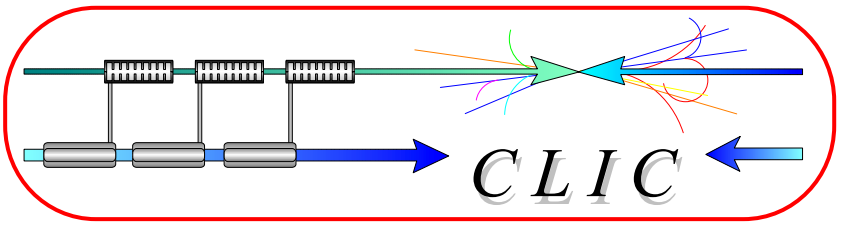

CLIC Note 504
PS/BD/Note 2001-015

CERN-OPEN-2002-010
25/01/2002

LASER WIRE SCANNER : BASIC PROCESS AND PERSPECTIVES FOR THE CTFS AND CLIC MACHINES

T. Lefèvre

Abstract

In a laser wire scanner, the basic idea is to replace the solid wire classically used in a standard wire scanner by a narrow laser beam. The basic process involved is the Thomson-Compton scattering process, where photons are scattered from the laser beam by the incoming electrons. By counting the number of scattered photons or degraded electrons as a function of laser position the bunch profile can be reconstructed. In this note the Compton scattering mechanism is first presented. In the framework of the CLIC project, a laser wire scanner (LWS) could be used as a non-interfering beam profile measurement both on the Drive Beam for a high current electron beam and on the Main Beam for very small electron beam sizes. A design for a LWS on the CTF2 and CTF3 machines is proposed and some considerations for the use of a LWS on the CLIC main beam are also mentioned.

Geneva, Switzerland
25 January 2002

Contents

Chapter 1

Motivation and review on Compton scattering

In a laser wire scanner, the basic idea is to replace the solid wire classically used in a standard wire scanner by a narrow laser beam. The process involved is the Thomson-Compton scattering process, where photons from the laser beam are scattered by the incoming electrons. By counting the number of scattered photons or degraded electrons as a function of laser position the bunch profile can be reconstructed. In the CLIC project, the characteristics of the electrons beams imply a new challenge in term of beam diagnostic performance. Classic profile monitors such as OTR screens or solid wire scanners would not be able to stand the high current of the Drive Beam (7.5A over $92\mu s$). Moreover, on the Main Beam line transverse sizes of the order of a micron would have to be measured, which represents a major challenge in terms of precision and fiability of the diagnostic. In this context laser wire scanners have certain advantages over classic diagnostics. They are non-destructive since they don't perturb the electron beam itself, they are non degradable, and they can be very accurate since the scanning precision depends mainly on the laser spot size which can be as small as a few wavelengths.

1.1 Introduction

In the late 19th century, J. Thomson discovered the scattering of an electromagnetic wave from a free electron at rest [1]. The electron is accelerated by the electric field and emits radiation in a direction other than that of the incident radiation. For very low photon energy ($h\nu_0 \ll m_e c^2$, with c the speed of light and m_e the electron mass), the frequency of the scattered photon, ν'_{sc}, is the same as the one of the incident photon ν_0.

When the incident photon energy is no more negligible with respect to the electron rest energy ($h\nu_0 \approx m_e c^2$), quantum mechanical effects modify the interaction and the effects of the electron recoil can not be ignored any more. This process, represented schematically in figure 1-1 has been demonstrated by Compton in 1923 [2] by measuring the kinetic energy E'_{sc} of the scattered electron. The kinematics were described in 1927 by Klein and Nishina [3]. These first observations were done using low energy electrons beam or electrons at rest and X-rays.

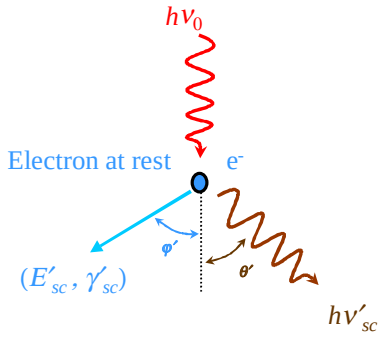

Figure 1-1: Elastic collision between a photon and an electron initially at rest

Using the conservation laws of energy and momentum, the energy of the scattered photon is defined by the following expression:

$$h\nu'_{sc} = h\nu_0 \left(\frac{1}{1 + \frac{h\nu_0}{m_e c^2}\left(1 - \cos(\theta')\right)} \right) \tag{1.1}$$

with θ' the scattering angle between the direction of propagation of the incident and the scattered photons. The energy of the scattered light is equal or lower than the incident photon energy. The kinetic energy of the scattered free electron and the corresponding scattering angle, noted φ', are given by :

$$E'_{sc} = \frac{(h\nu_0)^2}{m_e c^2}\left(\frac{1-\cos(\theta')}{1+\frac{h\nu_0}{m_e c^2}(1-\cos(\theta'))}\right) \text{ and } \varphi' = \arccos\left(\left(1+\frac{h\nu_0}{m_e c^2}\right)\tan\left(\frac{\theta'}{2}\right)\right) \tag{1.2}$$

The cross section of the Compton scattering process is given by the well-known Klein-Nishina [3] formula which describes the angular distribution of the scattered light (solid angle Ω):

$$\frac{d\sigma}{d\Omega} = \frac{r_e^2}{2}\frac{1}{\left(1+\frac{h\nu_0}{m_e c^2}(1-\cos(\theta'))\right)^2}\left(1+\cos^2(\theta')+\frac{\frac{h\nu_0}{m_e c^2}^2(1-\cos(\theta'))^2}{1+\frac{h\nu_0}{m_e c^2}(1-\cos(\theta'))}\right) \tag{1.3}$$

with r_e the classical electron radius ($r_e = \frac{e^2}{4\pi\varepsilon_0 m_e c^2} = 2.818 \cdot 10^{-15}\ m$), e the electron charge and ε_0 the permittivity of free space.

As shown by equations 1.1, 1.2 and 1.3, there is a correlation between the parameters of the scattered photons and electrons and the scattering angle θ'.

Integration of equation 1.3 over Ω gives the total cross section per electron for the occurrence of Compton scattering :

$$\sigma_c = 2\pi r_e^2\left[\frac{1+\xi_0}{\xi_0^3}\left[\frac{2\xi_0(1+\xi_0)}{1+2\xi_0}-\ln(1+2\xi_0)\right]+\frac{1}{2\xi_0}\ln(1+2\xi_0)-\frac{1+3\xi_0}{(1+2\xi_0)^2}\right] \tag{1.4}$$

with $\xi_0 = \frac{h\nu_0}{m_e c^2}$. One can note that for low energy photons, $\xi_0 \ll 1$, equation 1.4 reduces to the Thomson cross section defined by $\sigma_0 = \frac{8\pi}{3}r_e^2 = 6.65 \times 10^{-29} m^2$.

This theory is also valid for other particles such as protons and muons, provided one replace the electron mass by the corresponding particle mass in the equations .

1.2 Recent studies

During the second part of the 20th century, two major progresses in science have increased the interests in these processes : the development of accelerators allowing the production of relativistic electron beams, and the development of very high power lasers.

For the relativistic case, the Compton kinematic theory remains valid in the electron rest frame (noted with '). In the laboratory frame, the energy of the electromagnetic wave is affected by the relativistic Doppler shift. The ratio $h\nu_{sc}/h\nu_0$ becomes then directly proportional to γ_0^2, where $\gamma_0 = \left(1-\beta_0^2\right)^{-1/2}$ is the relativistic factor of the electrons, $\beta_0 = \frac{v_0}{c}$ with v_0 the electron velocity. The scattering angle is also affected by the relativistic contraction of length such that the scattered photons will be emitted in the forward direction, in a region of opening angle equal to $\frac{1}{\gamma_0}$. A representation of the interaction as seen in the laboratory frame, is shown in figure 1-2.

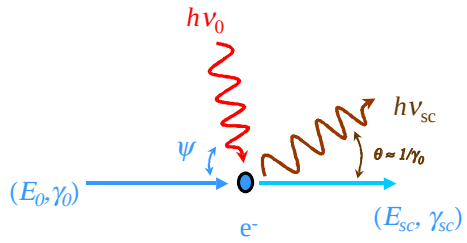

Figure 1-2: Relativistic Scattering process

The first proposal by Arutymian and Tumanian [5], and Milburn [6] of producing very high energy photons by colliding laser light with relativistic electrons dates back to the early 60's. Several experiments have also been performed to explore the possibility of using this process in electron diagnostics for accelerators [7] [8] and as a method of producing X-rays [9], [10], [11], [12] and [13]. As the rate of collisions increases linearly with the laser photon density $\langle n_0 \rangle$ (m^{-3}), with the actual high power laser sources [14]

the average number of scattered photons N_{sc}, reaches a level sufficiently high in order to be exploitable for different applications such as beam diagnostics. In a simple form, N_{sc} is given by the following expression

$$N_{sc} \approx \sigma_c \langle n_0 \rangle N_e D \tag{1.5}$$

where N_e is the number of electrons, D is the interaction length and $\langle n_0 \rangle$ is the average photon density at the interaction region defined by $\langle n_0 \rangle = \frac{1}{c \cdot h \cdot \nu_0} \frac{P}{S}$ with P the laser power, S the laser spot area.

Some studies have been done on the production of high peak fluxes of X-rays [15] based on head-on photon-electron collisions. The aim was to propose an alternative device, called Laser Synchrotron Source (LSS), to compete with the classical synchrotron light sources. At CERN, the ELFE project also proposes in its design to generate high energy γ-rays via Compton scattering.

1.3 General formulation of the Compton scattering process

1.3.1 Scattered photons and degraded electrons

In reference [17] a collision theory is derived in order to calculate the mechanics of the scattering process for relativistic beams. To study the interaction, the authors consider first the photon beam distribution in the laboratory frame. Then, using a Lorentz transformation, they compute the photon characteristics in the electron frame, where the Compton equations can be used. Finally, they came back to the laboratory frame, using an inverse Lorentz transformation obtaining the resulting scattered photons properties.

The energy of the scattered light can be expressed by

$$h\nu_{sc} = h\nu_0 \left(\frac{\gamma_0 m_e c^2 \left(1 - \beta_0 \cos(\psi)\right)}{\gamma_0 m_e c^2 \left(1 - \beta_0 \cos(\theta)\right) + h\nu_0 \left(1 - \cos(\psi - \theta)\right)} \right) \tag{1.6}$$

where ψ is the collision angle between the electron and the laser beam, θ is the observation angle of the scattered photons in the laboratory frame. The photon energy is maximum when emitted in the forward direction (i.e. $\theta = 0$) and it decreases rapidly as the observation angle moves away from that direction. By changing the collision angle, ψ, the energy of the scattered photons is also modified. The energy of the emitted photons in the forward direction goes from its minimum value equal to $\frac{h\nu_0\gamma_0 m_e c^2(1-\beta_0)}{\gamma_0 m_e c^2(1-\beta_0)+2h\nu_0} (\simeq h\nu_0$, i.e. no scattering $\psi = 0$) to the maximum value of $\frac{h\nu_0(1+\beta_0)}{(1-\beta_0)} (\simeq 4\gamma_0^2 h\nu_0)$ (head-on collision, $\psi = \pi$). For a 90 degree collision as in the case for a laser wire scanner, the maximum energy of the scattered photons is approximately $2\gamma_0^2 h\nu_0$.

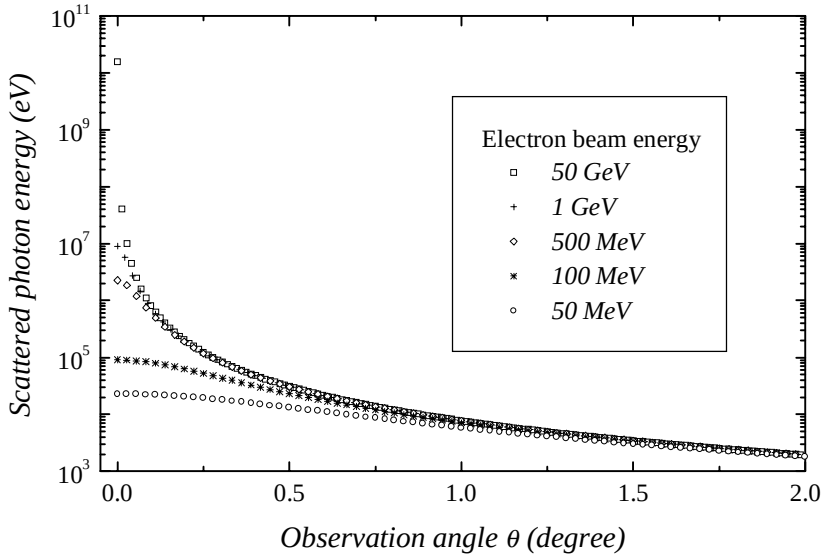

Figure 1-3: Scattered photons energy as a function of the observation angle.

In figure 1-3, the angular spectrum of the scattered light is calculated for different electron beam energies ranging from $50MeV$ to $50GeV$. Calculations are done using equation 1.6 and assuming a 90 degree collision with a $1.047\mu m$ wavelength laser beam (fondamental wavelenght of a Nd:YLF laser). As already mentioned, in the forward direction ($\theta = 0$), the ratio $\frac{h\nu_{sc}}{h\nu_0}$ is equal to $2\gamma_0^2$, so that at low energy ($50MeV$) $19keV$ soft X-rays are produced, whereas $15.6GeV$ γ-rays would result from a $50GeV$ electron beam. One can also note that for observation angles θ larger than $1°$, the curves are roughly the same and the energy of the scattered photons doesnot depend anymore on the electrons energy.

The spatial distribution of the scattered light, is given by the angular dependency of the Compton process cross section [4] :

$$\frac{d\sigma_c}{d\Omega} = \frac{\left(m_e c^2 r_e h\nu_{sc}\right)^2 \left(1 - \beta_0 \cos(\psi)\right)}{2\kappa_0^2} \left(\left[\left(m_e c^2\right)^2 \left(\frac{1}{\kappa_0} - \frac{1}{\kappa_1} \right) + 1 \right]^2 + \frac{\kappa_1}{\kappa_0} + \frac{\kappa_0}{\kappa_1} - 1 \right) \tag{1.7}$$

with $\kappa_0 = h\nu\gamma_0 m_e c^2 \left(1 - \beta_0 \cos(\psi)\right)$ and $\kappa_1 = h\nu_{sc}\gamma_0 m_e c^2 \left(1 - \beta_0 \cos(\theta)\right)$. Figure 1-4 shows the behavior of both the scattered photon energy and the cross section as a function of the observation angle. The calculation assumed a $40MeV$ electron beam, a $1.047\mu m$ ($1.16eV$) laser and a 90 degree collision angle. $14.8keV$ photons are emitted in the forward direction. In the literature [12] one considers that most of the scattered flux is confined into a cone of opening angle a few times the critical angle, α_c, defined by

$$\alpha_c = \frac{\sqrt{1 + 2\epsilon}}{\gamma_0} \tag{1.8}$$

with $\epsilon = \frac{\gamma_0 h\nu_0 (1 - \beta_0 \cos(\psi))}{m_e c^2}$. Only a tiny part of the incident laser light is scattered in the backward direction and its energy will be equal to $\frac{h\nu_0 \gamma_0 m_e c^2}{\gamma_0 m_e c^2 (1+\beta_0) + h\nu_0}$ ($\simeq \frac{h\nu_0}{2} = 0.58eV$).

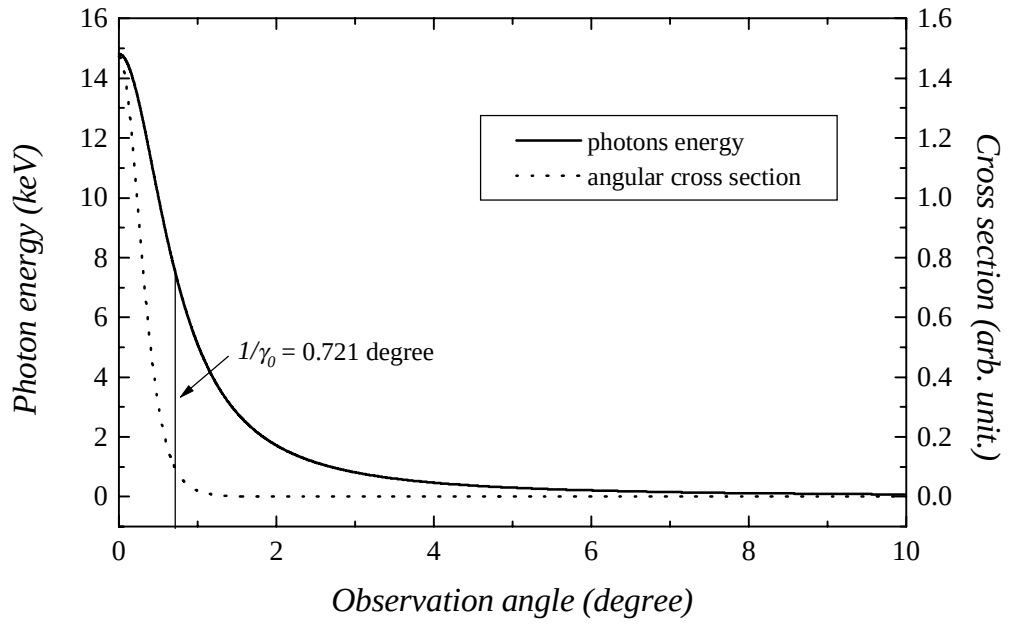

Figure 1-4: Evolution of the scattered photons energy and of the angular cross section as a function of the observation angle, calculated using equations 1.6 and 1.7.

Since, in this scattering process, the energy of the scattered X-rays is correlated to the scattering angle (see equation1.6), the energy spectrum of the scattered photons is given by

$$\frac{d\sigma_c}{dw} = \frac{3\sigma_0}{8\epsilon}\left(\frac{1}{1-w} + 1 - w + \left(\frac{w}{\epsilon\,(1-w)}\right)^2 - \frac{2w}{\epsilon\,(1-w)}\right) \tag{1.9}$$

where $w = \frac{h\nu_{sc}}{\gamma_0 m_e c^2}$ is the normalized X-rays energy.

The properties of the degraded electrons are calculated by employing the conservation laws of energy and momentum. First for a scattered photon of given energy, the energy of the corresponding degraded electron, noted E_{sc}, is obtained using the conservation law of energy. Secondly, equation 1.6 shows that the energy of the scattered photon is correlated

to its scattering angle θ. As both the characteristics of the scattered photon (energy and angle) and the degraded electron energy are known, the scattering angle of the degraded electron, denoted φ, can be deduced from the conservation law of momentum. In the laboratory frame E_{sc} and φ are then given by

$$E_{sc} = \gamma_0 m_e c^2 + h(\nu_0 - \nu_{sc}) \tag{1.10}$$

$$\varphi = \arccos\left[\frac{\gamma_0 m_e \beta_0 c - \frac{(h\nu_0\cos(\psi)+h\nu_{sc}\cos(\theta))}{c}}{\gamma_{sc} m_e \beta_{sc} c}\right] \tag{1.11}$$

1.3.2 From Thomson to Compton regimes

In the Thomson regime (low energy electrons and photons), equation 1.6 is reduced to

$$h\nu_{sc} = \frac{h\nu_0\,(1 - \beta_0\cos(\psi))}{(1 - \beta_0\cos(\theta))} \tag{1.12}$$

To illustrate the limit between the Thomson and Compton regimes, the scattered photon energy was calculated using the two corresponding formulas 1.6 and 1.12. On figure 1-5 the energy of the scattered photons is plotted as a function of the observation angle for two different electron beam energies (1 and $50GeV$) using a $1.06\mu m$ laser and a 90 *degree* collision angle. At $1GeV$, the maximum photon energy ($\theta = 0$) is equal to $9MeV$ and the difference between the two models is very small ($80keV$). At higher energy the difference becomes larger, and at $50GeV$, the maximum photon energy is $15.59GeV$. The discrepancy between the two formulas represents 50% of this value and arises from the fact that in the Thomson theory the electron recoil is not taken into account. So, in the analysed case (using IR laser light), for electron beam energy above $1GeV$, quantum effects become important and the Thomson formulas can not be used anymore.

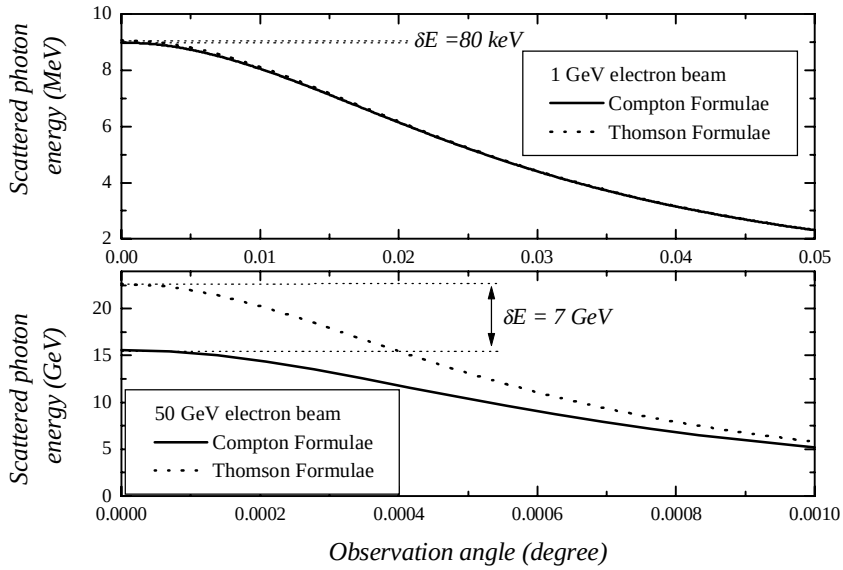

Figure 1-5: Angular spectrum for a 90 degree collision between an infrared laser beam and a 1 GeV (above) and 50 GeV (below) electron beam as observed in the laboratory frame.

1.4 Laser Wire scanner experiments

Several schemes have been proposed, and both 90 degree Thomson [18] and Compton [19] scattering have been considered to serve as diagnostic for bunch length and beam profile measurement. The laser beam is used as a probe to scan either the electron bunch length (assuming that the laser pulse duration is shorter than the electron bunch duration, the scan is achieved by delaying the laser pulse along the bunch length) or the electron beam transverse distribution (assuming that the RMS laser beam size is lower than RMS transverse electron beam size).

Such experiments on laser wire scanners have been performed in 1996 both at the Advanced Light Source (ALS) at the Lawrence Berkeley national Laboratory (LBNL) [20] and at the Final Focus Test beam at SLAC [21] [22]. At LBNL, the set-up consisted

of a $50MeV$ electron beam provided by the ALS injector, and a high power Ti:Al2O3 laser beam delivering terawatt femtosecond pulses. The second experiment has been performed at SLAC on a $50GeV$ electron beam using a medium power Nd:YLF laser. All the experimental data are summarized in the table 1.

Parameters	**LBNL**	**SLAC**
Beam energy (MeV)	*50*	*50000*
Bunch charge (nC)	*1.3*	*1.6*
Bunch length (μm)	*3000*	*2000*
Beam transverse size (μm)	*100*	*1*
Laser type	*Ti : Al2O3*	*Nd : YLF*
Laser Wavelength (nm)	*800*	*349(x3)*
Laser Energy (mJ)	*40*	*0.025*
Laser Power (GW)	*400*	*0.01*
Laser focused waist (μm)	*30*	*0.5*
Angle of collision	*$\pi/2$*	*$\pi/2$*
Laser Pulse duration (ps)	*0.1*	*2.5*
Maximum energy of scattered photons	*30keV*	*29GeV*
Diagnostic Type	*X-rays*	*e^-, X-rays*
Half angle of the emission cone θ_c (rad)	*0.01*	*$2.5 \cdot 10^{-5}$*
Number of scattered photons per bunch	*$5 \cdot 10^4$*	*5000*

Table 1 : Results from previous experiments at LBNL and SLAC

At LBNL, a $5 \cdot 10^4$ X-rays flux was measured using both Germanium detectors in counting mode and phosphor screens for imaging. At SLAC both the degraded electrons and the scattered γ-rays were measured using scintillators.

Recently, a laser wire scanner was installed on the electron damping ring at the Accelerator Test Facility at KEK [23]. In their scheme, they produced Compton scattering on

a $1.54GeV$ electron beam circulating in a storage ring by injecting a CW $(50mW, 532nm)$ laser light into a fabry-perot optical cavity installed on the beam path. The scanning system was achieved mechanically by displacing a movable table supporting the laser, allowing a position resolution better than $1\mu m$. The signal to noise ratio is extremely low of the order of $1/5$, and the good shielding of the detector was of great importance.

1.5 Non linear and multiple scattering process

Initially we considered the interaction of a single photon with a single electron (called linear process). Using very high power light sources, more than one photon can interact with the same particle and in this case, two different processes can be observed as shown on figure 1-6.

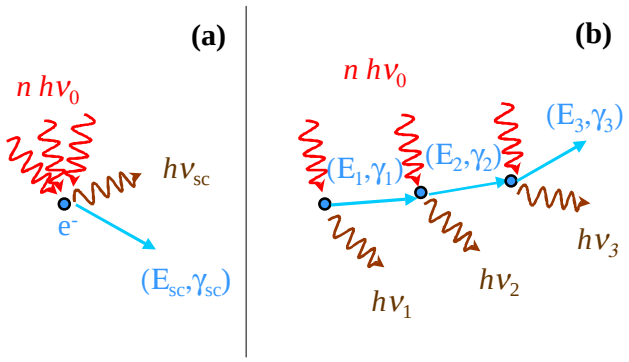

Figure 1-6: Scattering process using very high power laser. (a) Non linear scattering. (b) Multiple scattering.

The first one is called non linear scattering (a), and corresponds to the absorption of several photons accompanied by emission of a single photon of higher energy corresponding to harmonic emission. The second one (b) is the multiple scattering scheme and

it can be seen as several linear scattering interaction experienced by the same electron one after the other. E1, E2 and E3 are the consecutive energies of the electron which is experiencing three consecutive collisions.

At SLAC, non linear Compton scattering has been observed in the collision of a low emittance $46.6GeV$ electron beam with a $1.5ps$ chirped-pulsed-amplified Nd:glass terawatt system delivering $800mJ$ at $1054nm$. They have detected scattered photons corresponding to second third and fourth harmonic emission [26].

One can also notice that in non linear scattering process, the frontier between the Thomson and Compton regimes can be reached by increasing the laser power density. Such measurements have been recently done using low energy electrons (keV) by measuring the energy variation of the electron passing through the laser focus [27]. Initially in the Thomson regime, electrons don't loose a significant part of their energy during the interaction, but when several photons collide with the same electron the corresponding energy loss is no longer negligible and can be detected. A theory of this non linear Thomson scattering process is presented in reference [24], and a review on such studies can be found in reference [25].

Chapter 2

Laser Wire Scanner

2.1 Experimental layout and interaction zone

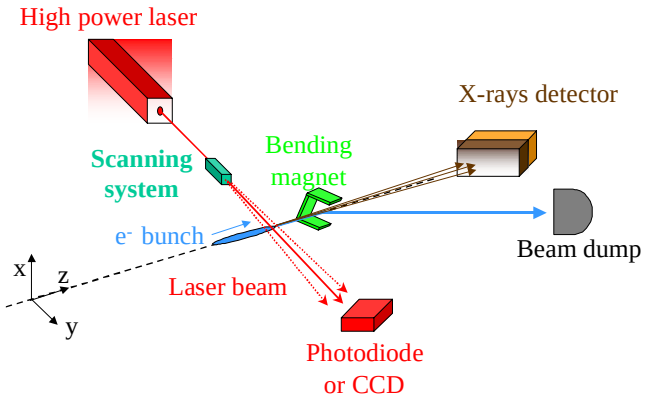

Figure 2-1: Laser Wire scanner experimental setup

The experimental layout is shown on figure 2-1. In a laser wire scanner, a 90 degree collision angle between the laser and the electron beams is used. The laser beam is strongly focused at the interaction point with the aim of obtaining a beam waist much

smaller than the transverse size of the electron beam. A deflecting system is used to scan the laser beam through the electron beam. The scattered photons, X-rays in our case, are emitted within a small solid angle in the forward direction. To make their detection possible, the electron beam must be deflected using a bending magnet. This kind of detection system on linear accelerators can only be used with low energy electron beams. At higher energies, problems arise when trying to bend the particles. Moreover, the detection of high energy γ-rays will become more complicated and no longer compatible with the geometry of a linear accelerator. On the other hand, when the electron energy becomes sufficiently high, such as it is foreseen for the CLIC main beam, the electrons will loose a significant portion of their energy in their collision with the laser photons and the resulting degraded electrons can be detected instead.

The close-up view of the interaction region is shown on figure 2-2. Let's consider here that both the laser and the electron beams are of gaussian shape. The laser beam, supposed to be round, is described by the following parameters: σ_L is its RMS pulse length and σ_w is its RMS transverse width at the waist position. One may note that σ_w corresponds to one half of the waist size, ω_0, in the laser terminology. The Rayleigh range [28], Z_R, is defined to be the distance over which the laser waist size increases by a factor of $\sqrt{2}$. This parameter is particularly important in order to estimate how rapidly an ideal gaussian beam will expand due to diffraction spreading as it propagates away from the waist region. The electron bunch is defined by its RMS pulse length σ_z and respectively its x and y RMS transverse widths $\sigma_{x,y}$.

For an explicit calculation , the laser and the electron beams are supposed to propagate along the y and z direction respectively. The intensity of the laser beam taken at a time t, is given by

$$I(x,y,z,t) = I_0 \exp\left(-\frac{1}{2}\left[\frac{(y-ct)^2}{\sigma_L^2} + \frac{x^2+z^2}{\sigma_w^2}\right]\right) \tag{2.1}$$

Assuming that the electron trajectories are parallel to the z axis, the intensity felt by a

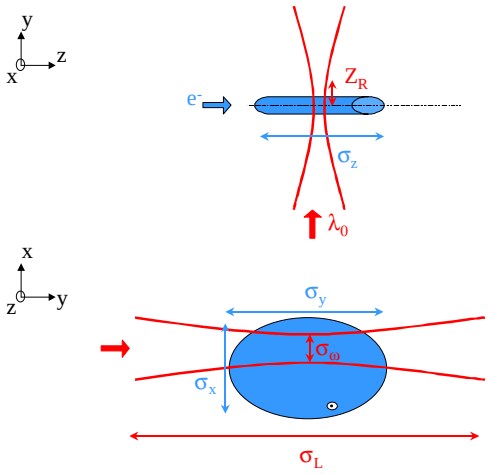

Figure 2-2: Close up of the laser-electron beams interaction zone.

single electron can be written as follows [18]

$$I_i(x,y,z,t) = I_0 \exp\left(-\frac{1}{2}\left[\frac{(t-t_i)^2 - t_i^2}{\tau^2} + \frac{y_i^2}{\sigma_L^2} + \frac{x_i^2+z_i^2}{\sigma_w^2}\right]\right)$$

with $\tau = \frac{\sigma_L \sigma_w}{c\sqrt{\sigma_L^2+\sigma_w^2}}$ the duration of the field seen by the electron and $t_i = c\sigma_\tau^2\left(\frac{y_i}{\sigma_L^2} + \frac{z_i}{\sigma_w^2}\right)$.

The function $I_i(t)$ is of a gaussian shape with an RMS width τ, so that by integrating over t, the effective interaction length, L_i, can be expressed by

$$L_i = \sqrt{2\pi} c\tau$$

If the laser pulse length is large compared to the waist size, the interaction length L_i becomes equal to the transverse dimension of the laser waist ($\sqrt{2\pi}\sigma_w$ for a gaussian beam).

The number of electrons, N_e, contained in the volume $dx_i dy_i dz_i$ is given by:

$$f(x_i,y_i,z_i)dx_i dy_i dz_i = \frac{N_e}{(2\pi)^{\frac{3}{2}}\sigma_x\sigma_y\sigma_z}\exp\left(-\frac{1}{2}\left[\frac{z_i^2}{\sigma_z^2} + \frac{x_i^2}{\sigma_x^2} + \frac{y_i^2}{\sigma_y^2}\right]\right) dx_i dy_i dz_i \qquad (2.2)$$

2.2 Calculation of the number of scattered photons

To quantify the interaction, two different approaches are currently used. The first one is based on the collision process [17] considering the laser source as particle of light. The second one [18] is derived from the synchrotron theory in which the laser light is associated to an electromagnetic wave and compared to a static undulator. Both theories are presented in this section and their results are compared.

2.2.1 Collision theory

In the specific case of a LWS, the collision angle is set to $\frac{\pi}{2}$. The general equation 1.6 is then simplified and, the scattered photon energy can be written

$$(h\nu_{sc})_{\max} = h\nu_0 \left(\frac{\gamma_0 m_e c^2}{\gamma_0 m_e c^2 \left(1 - \beta_0 \cos\theta\right) + h\nu_0 (1 - \sin\theta)} \right) \tag{2.3}$$

with a maximum value of $\frac{h\nu_0}{(1-\beta_0)}$ for θ equal to zero.

A simple formula has also been defined in equation 1.5 in order to give an estimate of the total number of scattered photons produced during an electron-laser beam collision. Considering the laser and the electron beam distributions described in 2.1 and 2.2, this formula is modified, and the number of photons scattered into a given spectral width $\Delta\lambda/\lambda$ can be re-written after integration over $dx_i dy_i dz_i dt$ as follows

$$(N_{sc})_{col} = \sqrt{2}\sigma_c N_e \left(\frac{P}{2\pi\sigma_w^2} \right) \frac{L_i}{ch\nu_0} \left(\frac{\Delta\lambda}{\lambda} \right) \frac{\sigma_w \sqrt{\sigma_L^2 + \sigma_w^2}}{\sqrt{\left(\sigma_x^2 + \sigma_w^2\right)\left(\sigma_z^2 + \sigma_y^2 + \sigma_L^2 + \sigma_w^2\right)}} \tag{2.4}$$

where N_e is the total number of electrons contained in the beam

Using the definition of L_i, equation 2.4 becomes finally,

$$(N_{sc})_{col} = \sqrt{2}\sigma_c N_e \frac{P}{ch\nu_0} \left(\frac{\Delta\lambda}{\lambda} \right) \frac{\sigma_L}{\sqrt{\pi\left(\sigma_x^2 + \sigma_w^2\right)\left(\sigma_z^2 + \sigma_y^2 + \sigma_L^2 + \sigma_w^2\right)}} \tag{2.5}$$

2.2.2 Synchrotron light emission analogy

In that scheme [18], let's consider that the electric field associated with the laser beam is in the direction perpendicular to the scattering plane. Its peak amplitude E_0 is expressed in term of laser power density $\frac{dP}{dA}$ as follows

$$E_0 = \sqrt{2Z_0 \frac{dP}{dA}}$$

where $Z_0 = 377\Omega$ is the free space impedance. The laser beam is equivalent to a static magnetic undulator with a peak magnetic field B_0 and a period length λ_u defined by

$$B_0 = \frac{E_0}{c}\left(1 - \beta_0 \cos(\psi)\right) \quad \text{and} \quad \lambda_u = \frac{\lambda_0}{\left(\frac{1}{\beta_0} - \cos(\psi)\right)}$$

For an undulator it is convenient to introduce the deflection parameter $K = \frac{eB_0\lambda_u}{2\pi mc}$. The radiation characteristics from an undulator are well known [32] and the emitted spectrum has a peak at

$$(\lambda_{sc})_{\max} = \frac{\lambda_u}{2\gamma^2}\left(1 + \frac{K^2}{2}\right) \tag{2.6}$$

In most of the cases, the factor K is quite low and the corresponding term in the equation 2.6 can be ignored. However, for very high power laser, its contribution becomes significant.

As a first approximation, the number of photons emitted by a single electron into a given spectral width $\Delta\lambda/\lambda$ is then given by [32]

$$(N_{sc})_e = \pi\alpha K^2 N_{eff}\frac{\Delta\lambda}{\lambda}$$

where $\alpha \cong 1/137$ is the fine structure constant and $N_{eff} = \frac{L_i}{\lambda_u}$ is the effective number of undulator periods experienced by the electrons.

To calculate the total number of scattered photons in a more realistic case, one can use the laser and electron beam distributions respectively defined by equations 2.1 and 2.2. The number of photons generated by the i^{th} electron that passes through the $z = 0$ plane per time unit can therefore be written

$$\frac{d\left(N_{sc}\right)_i}{dt} = \pi\alpha K^2 N_{eff}\left(\frac{\Delta\lambda}{\lambda}\right)\delta\left(t - z_i/c\right)\exp\left(-\frac{1}{2}\left[-\frac{t^2}{\tau^2} + \frac{y_i^2}{\sigma_L^2} + \frac{x_i^2 + z_i^2}{\sigma_w^2}\right]\right) \tag{2.7}$$

where $\tau = \frac{\sigma_L\sigma_w}{c\sqrt{\sigma_L^2+\sigma_w^2}}$ represents the duration of the magnetic field experienced by an electron. The number of photons, N_{sc}, scattered out by the electron beam is then obtained by multiplying equations 2.7 and 2.2, and integrating over $dx_i dy_i dz_i dt$. One finally obtains

$$\left(N_{sc}\right)_{syn} = 2\pi^{3/2}\alpha K^2 N_e\left(\frac{\Delta\lambda}{\lambda}\right)\frac{\sigma_L\sigma_w^2}{\lambda_u\sqrt{\left(\sigma_x^2+\sigma_w^2\right)\left(\sigma_z^2+\sigma_y^2+\sigma_L^2+\sigma_w^2\right)}} \tag{2.8}$$

where N_e is the total number of electrons contained in the beam.

The RMS pulse duration of the X-ray beams is given by

$$T = \frac{\sigma_z\sqrt{\sigma_y^2+\sigma_L^2+\sigma_w^2}}{c\sqrt{\sigma_z^2+\sigma_y^2+\sigma_L^2+\sigma_w^2}} \tag{2.9}$$

Using the parameters of the LBNL experiment which are given in table 1, the numerical values given by the two approaches are calculated. For the calculations, the spectral band $\frac{\Delta\lambda}{\lambda}$ is equal to 0.7, so that the number of scattered photons corresponds to the ones collected in the $5mrad$ detection angle they used.

$$\left(N_{sc}\right)_{col} = 6.46\cdot 10^4 \text{ and } \left(N_{sc}\right)_{syn} = 6.87\cdot 10^4$$

The results are quite similar with a difference of 6%. In this experiment $5\cdot 10^4$ X-rays photons were measured. The sensitivity of the detector and the angular dispersion of the scattered photons beam could be responsible for that difference.

2.2.3 Case of an off centered collision

The formula given in the two previous paragraphs are considering that both the electron and the laser beam distribution are centered at the same position. This situation corresponds to the best spatial overlap which gives the highest rate of events. If one introduces an offset Δx, between them, the number of scattered photons will decrease, the electrons will not experience the maximum photon density anymore, and Δn will become

$$N_{sc}(\Delta y) = (N_{sc})_{col,syn} \exp(-\frac{\Delta x^2}{2\,(\sigma_x^2 + \sigma_w^2)}) \tag{2.10}$$

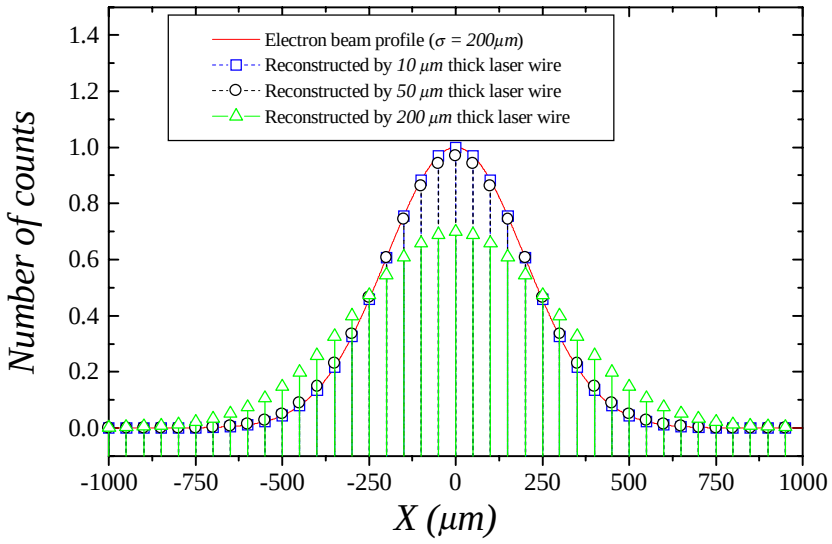

Figure 2-3: Transverse profile of a $200\mu m$ electron bunch measured with a laser wire scanner. Each curve corresponds to a different laser spot size.

Using this formula one can determine the electron profile that would be obtained with a laser wire scanner. In figure 2-3 several curves are plotted representing the bunch profile measured with a laser wire of respectively 10, 50 and 200 μm of transverse width. The

measurement is based on the convolution of both the laser and the electrons transverse width (here 200 μm). So since the laser spot size is kept small (here $<50\mu m$) with respect to the electrons beam size, the measured profile fits very well to the electron bunch profile. But when the laser size increases too much, the measured profile is increased too, and one must take into account this effect to get the real transverse width of the electrons bunch. The number of counts, which is proportional to the laser power density decreases also when the laser spot size increases.

2.2.4 Spectral broadening

Equation 1.6 shows that there is a correlation between the scattered photons energy and the observation angle, the photons of maximum energy being scattered in the forward direction. At first, our treatment supposes that the electron beam is monoenergetic and the spectral width of the laser is negligible. In that case, the natural spectral broadening of the process $\left(\frac{\Delta\nu}{\nu}\right)_n$ at a fixed observation angle θ is only due to the finite dimension of the interaction length [15].

$$\left(\frac{\Delta\nu}{\nu}\right)_n = \frac{\lambda_u}{L_i} \tag{2.11}$$

where λ_u is the undulator period defined in the previous paragraph.

The spectral width $\left(\frac{\Delta\nu}{\nu}\right)_E$ due to the electron beam energy spread is obtained using equation 2.3 :

$$\left(\frac{\Delta\nu}{\nu}\right)_E = \frac{1+\frac{\beta\gamma h\nu_0}{mc^2}}{\beta\gamma^2\left(1-\beta+\frac{h\nu_0}{\gamma mc^2}\right)}\frac{\Delta E}{E_b} \tag{2.12}$$

For relativistic electrons, $\beta \approx 1$, $\gamma \gg 1$ and equation 2.12 reduced to $\left(\frac{\Delta\nu}{\nu}\right)_E \simeq \frac{\Delta E}{E_b}$. This formula is only valid for a 90 degree scattering, and will be multiplied by a factor of 2 if considering a head-on collision.

Moreover, realistic electron beams have an average angular spread as well as an average energy spread, and these imperfections increase the spectral width of the scattered beam. The electron beam emittance and the intrinsic energy spread, $\left(\frac{\Delta E}{E_b}\right)_{E_{in}}$, associated with the electron beam will account for the angular and energy spreads respectively. The normalized beam emittance is given by $\varepsilon_n = \gamma_0 r_b \theta_b$, where r_b is the average beam radius and θ_b is the average electron angular spread. The fractional longitudinal beam energy spread due to emittance is [15]

$$\left(\frac{\Delta E}{E_b}\right)_{E_{\varepsilon_n}} = \frac{\varepsilon_n^2}{2r_b^2}$$

where E_b is the initial electron beam energy.

The total spectral width of the radiation is

$$\left(\frac{\Delta\nu}{\nu}\right)_T \simeq \sqrt{\left(\frac{\Delta\nu}{\nu}\right)_n^2 + \left(\frac{\Delta\nu}{\nu}\right)_{E_{\varepsilon_n}}^2 + \left(\frac{\Delta\nu}{\nu}\right)_{E_{in}}^2} \tag{2.13}$$

and the total radiation is mainly confined in a solid angle of half angle, θ_T, defined as follows

$$\theta_T \approx \frac{\sqrt{\left(\frac{\Delta\nu}{\nu}\right)_T}}{\gamma_0} \tag{2.14}$$

Recently [33] a 3D simulation code has been developed to study the influence of the energy dispersion and the emittance of the electron beam on the luminosity of the scattered light .

2.3 Laser focusing system

2.3.1 Geometrical optic and diffraction limited spot size

In classical laser theory [28], which is based on the diffraction limit assuming that the laser spot size is always larger than the laser wavelength ($\omega_{diff} > \lambda_0$), the waist size of the laser beam ω_{diff} passing through a lens is given by:

$$\omega_{diff} = \frac{\lambda_0 f}{\pi \omega_{ini}} \tag{2.15}$$

where f is the focal length of the lens and ω_{ini} is the laser radius at the lens position. To achieve very small sizes, one has to use either short wavelengths or lenses with short focal length and big radius in order to allow an initial laser spot size ω_{ini} as large as possible. In practice, ω_{ini} is limited by the laser transport and the size of the focusing lenses.

To characterize the laser focus, it is also important to consider the Rayleigh range Z_R, which represents the length over which the laser beam is kept focused ($\omega = \sqrt{2}\omega_{diff}$). Z_R is given by

$$Z_R = \frac{\pi \omega_{diff}^2}{\lambda_0} \tag{2.16}$$

The effective length of the laser focusing, L_g, is twice the Rayleigh range.

The requirements for the focus of a laser wire scanner are imposed by the parameters of the electron beam to be analyzed. Let's consider an electron beam with transverse dimensions, σ_x and σ_y, and suppose the scanning is done on the y axis. The laser spot size ω_{diff} must be much smaller than σ_y so that the electron beam profile can be reconstructed by scanning the laser through the beam. Moreover ω_{diff} must remain constant over a distance equal or larger than σ_x ($L_g > \sigma_x$) to avoid smearing the results.

In the following paragraph, two extreme cases have been considered. They correspond to the CLIC main beam parameters ($1.5TeV$) and to the CTF2 beam ($40MeV$). The

CLIC main beam will have very small beam sizes (sub micrometer range) with σ_y 100 times smaller than σ_x. On CTF2, using a quadrupole triplet to focus the electrons, one should be able to obtain a round beam of $200\mu m$ transverse RMS size. Using equations 2.15 and 2.16, the required laser wavelength and focusing lenses have been calculated, and the results are given in table 2.

Parameters	**CTF2**	**CLIC**		
Beam energy	*40MeV*	*1.5TeV*		
Beam transverse size σ_x (μm)	*200*	*40*		
Beam transverse size σ_y (μm)	*200*	*0.4*		
Laser waist spot size ω_{diff} (μm)	*38*	*0.25*		
Lens focal length f (mm)	*200*	*10*		
Laser wavelength (nm)	*1047*	*250*	*100*	*10*
Laser spot size ω_{ini} (mm)	*1.8*	*3.18*	*1.27*	*0.13*
Effective length of the laser focusing (μm)	*8300*	*1.57*	*3.93*	*39.27*

Table 2: Laser focusing requirements for CTF2 and CLIC main beam

For the case of CTF 2, the laser focusing is not critical. A $40\mu m$ laser spot size should be sufficient to scan a $200\mu m$ electron beam and it is achieveable using a classic laser source (for example using the infrared light from a YLF or a YAG laser) and a $200mm$ focal length lens. The corresponding $8.3mm$ distance over which the laser beam remains focused is large enough to provide a good measurement.

For the CLIC main beam, the electron beam dimensions are much smaller, so that one has to consider a laser with a much shorter wavelength and focusing lens with a shorter focal length too. The goal of these calculations is just to indicate how critical the laser focusing is. A $10mm$ focal length lens has been chosen, which is quite realistic and is also compatible with the size of the beam pipe ($4mm$ diameter) in the CLIC main linac. 3 different laser wavelengths from $250nm$ (which corresponds to the fourth harmonic of

a YLF laser) to $10nm$ have been considered in the calculations. The laser spot size has been fixed to $250nm$ which, being quite optimistic, represents the minimum size of the diffraction limited $250nm$ wavelength laser. The results show that with the $100nm$ and moreover with the $250nm$ wavelength laser, the effective lengths of the laser focusing, respectively of 3.93 and $1.57\mu m$ are not long enough to provide a clean measurement over the σ_x beam dimension. In order to meet that requirement, a $10nm$ wavelength laser source would be needed, but unfortunately does not exist yet.

In the calculation presented in table 2, the focal length has been chosen arbitrarily. Since the laser waist size, ω_{diff}, is fixed by the parameters of the electron beam and must remain unchanged (for example $250nm$ for the CLIC main beam), other designs allowing a larger ω_{ini} spot size on the focusing lens can be foreseen using a lens with a longer focal length. This modification doesn't have any effects on the focusing effective length, L_g, which will remain the same since ω_{diff} and λ_0 stay unchanged. For a $250nm$ laser wavelength, using respectively a $5cm$, $10cm$ and a $20cm$ focal length lens, the corresponding values of ω_{ini} will be respectively of $1.592cm$, $3.183cm$ and $6.36cm$. This will imply a modification of the geometry of the interaction chamber since the size of the optics has to be adapted to these focusing requirements. An important issue of the design comes also from the fact that the parameters of the focusing system (focal length, lens diameter) have to be compatible with the use of high power laser. This means that the laser spot size, ω_{ini}, on the focusing lens should be large enough to avoid damaging the lens itself in a long term operation of the diagnostic.

In a real system, the focus of light is not only limited by diffraction but also by the spherical aberration of the system. The spot size due to aberration is given by

$$\omega_{sph} = \frac{k\omega_{ini}^3}{f^2} \tag{2.17}$$

so that the real spot size is given by the sum of the diffraction and spherical aberration

limited spot size.

$$\omega_0 = \omega_{diff} + \omega_{sph} \tag{2.18}$$

The contribution of aberrations can be minimized by using aspheric lenses or parabolic mirrors. Anyway to be predictible, the minimum achievable spot size of a given system has to be determined carefully by ray tracing using a simulation code like ZEMAX [29]. In the framework of the Laser Wire Scanner studies, these simulations are performed by RHUL and will be presented later.

2.3.2 Optical system and interaction chamber

A possible design of the interaction vacuum chamber is given on figure 2-4. Two vacuum windows have to be inserted to let the laser pass through beam tube. The distance between the focussing lens and the viewports must be set to minimize the laser power density on the viewport itself to prevent for any damage. The re-imaging system is located out of beam tube (lens and light attenuator) and a CCD camera should be used to monitor the laser light after the interaction region.

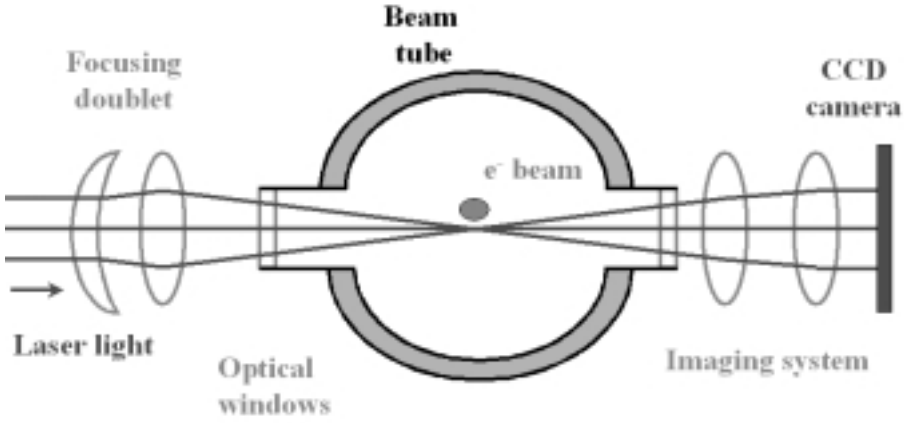

Figure 2-4: Drawing of the interaction chamber and of the laser focusing and imaging systems

To achieve a diffraction limited spot size, the focusing system (lens or parabolic mirror) must be inserted inside the vacuum minimizing the diffusion on the vacuum window. Different ways of scanning the laser beam such as the use of mechanical (piezoelectric) or electro-acoustic micro-movable device have to be studied and developed. At KEK[23], they have implemented a LWS where the laser system is put onto a micromovable optical table, and the scanning is done by moving up and down the whole table, achieving a $1\mu m$ spatial resolution.

Chapter 3

LWS for CTF 2

In order to demonstrate the feasibility of the Compact LInear Collider (CLIC) project, several experiments have been performed on the CLIC Test Facilities (CTF). CTF 2 [34] has demonstrated the energy transfer with the so called Two Beam Acceleration scheme. Currently, CTF 2 is used to test some of the key components of the CLIC Project, such as the accelerating structures [36] and new diagnostics [37]. Investigations on coherent synchrotron radiation in a magnetic chicane have been studied [38] are also pursued on CTF 2.

We are investigating the possibility of using CTF2 for characterizing the Thomson scattering process and for developing appropriate X-ray detectors. Table 3 shows a summary of the main characteristics of the electron beams produced in CTF 2 (Drive Beam=DB and Probe Beam=PB).

Parameters	**CTF II DB**	**CTF II PB**
Beam energy (MeV)	*40*	*45*
Bunch charge (nC)	*13*	*1*
Number of electrons per bunch	$8 \cdot 10^{10}$	$6.25 \cdot 10^{9}$
Bunch length (ps) FWHM	*2-10*	*10*
Number of bunches / *Bunch spacing (cm)*	1 - 48 / *10*	*single bunch*
RMS Beam Size $\sigma_y(\mu m)$	*150*	*150*
Normalised RMS emittance $(\pi.mm.mrad)$	*150*	*70*
Energy spread (%)	*4*	*10*
Desired waist size σ_w (μm)	*50*	*50*
Repetition rate (Hz)	*5-10*	*5-10*

Table 3: Characteristics of the electron beams available on CTF 2

An interesting point is that the CTF 2 photoinjector is driven by a high power Nd:YLF laser. The initial power at the nominal wavelength ($1047nm$) is used to produce the UV light dedicated to the electron photoemission. After the frequency conversion process, a large amount of infrared light is still available. We propose here to use this unused laser power either at $1047nm$ ($2.5mJ, 100MW$) or at $523nm$ ($0.5mJ, 20MW$) to serve as the laser probe in the LWS. These values take into account a 50% energy loss in the optical line to transport the laser beam to the collision zone. Preliminary calculations have been done and the results are shown in table 4 for the drive beam and in table 5 for the probe beam. The drive beam calculations have been done using a $13nC$ electron bunch and considering a $10mrad$ detection angle.

Parameters	$\boldsymbol{\lambda_0}$**= 1.047**$\boldsymbol{\mu}$**m**	$\boldsymbol{\lambda_0}$**= 523nm**
Maximum X-rays energy (keV)	*15*	*30*
Half angle of the emission cone θ_T *(mrad)*	*9*	*9*
Total Number of emitted photons per bunch (N_{sc})	$2.4 \cdot 10^4$	*2400*

Table 4: Thomson scattered light produced with the drive beam.

Parameters	λ_0= **1.047μm**	λ_0= **523nm**
Maximum X-rays energy (keV)	*19keV*	*38keV*
Half angle of the emission cone θ_c (mrad)	*3.7*	*3.7*
Number of emitted photons per bunch (N_{sc})	*2300*	*230*

Table 5: Thomson scattered light produced with the probe beam :

The available laser power in the green light is lower than in the IR, so that the number of collisions is also lower. From that point of view, using IR is a better solution for CTF2.

As mentioned before, the number of scattered photons evolves proportionally to the number of electrons. The CTF 2 drive beam has the capability to produce a single bunch where the bunch charge can be set from 1 to $100nC$. On figure 3-1 the number of scattered photons N_{sc} is plotted as a function of the bunch charge Q_b. Calculations have been made using different laser transverse sizes of $10\mu m$, $30\mu m$ and $50\mu m$.

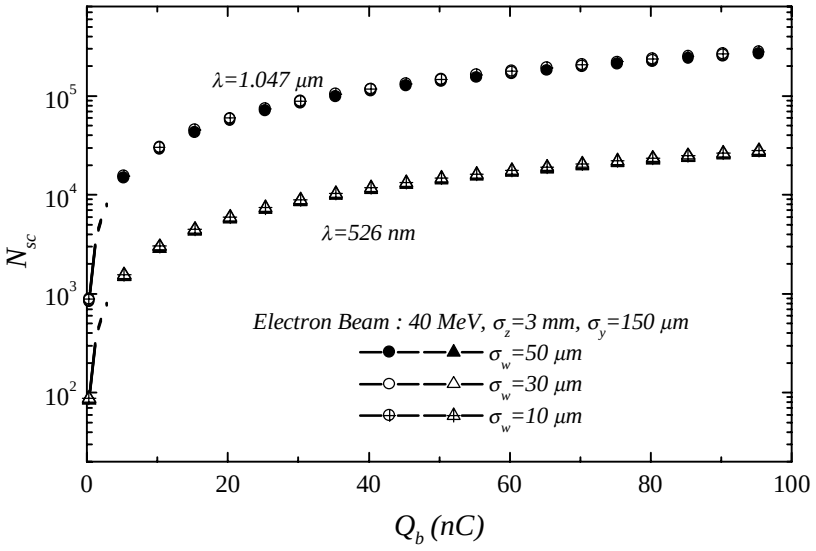

Figure 3-1: Evolution of the number of scattered photons as a function of the bunch charge

On figure 3-2, the number of events is plotted as a function of the transverse electron beam size ($13nC$ bunch). No significant difference can be observed when using different laser spot size. The number of scattered photons decreases as the electron beam size increases so that for electron transverse sizes above $400\mu m$, the number of scattered X-ray photons go down to 10^4 and 10^3 respectively for infrared and green light.

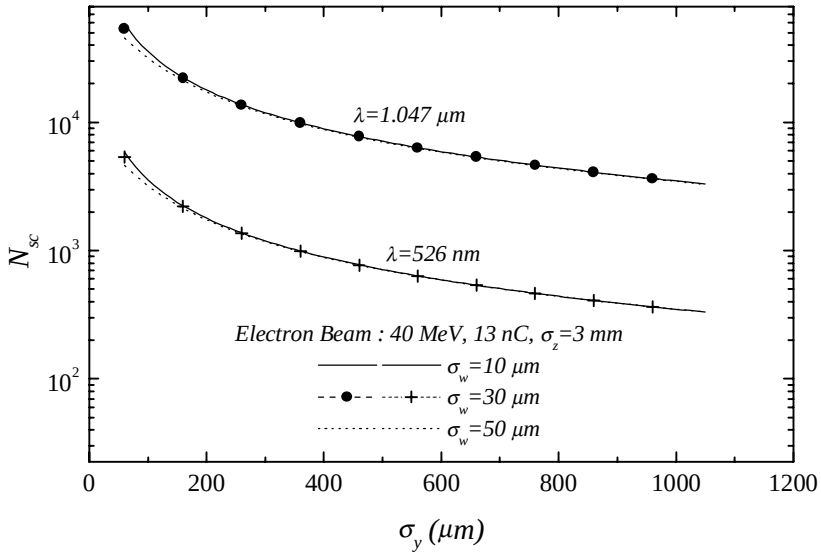

Figure 3-2: Evolution of the number of scattered photons as a function of the electron RMS transverse size

Chapter 4

LWS for CTF 3

CTF 3 [40] is the new CLIC Test Facility presently under construction with the aim of demonstrating the production of a 30 GHz drive beam using a 3 GHz linac and combiner rings. The first electron beam has been produced in September 2001. Progressive phases of beam operation have been planned in the following five years. The preliminay phase will reuse most of the existing part of the LIL linac and the beam current will be relatively low. The nominal phase will start in 2003, and the design of the linac will be completely modified in order to be adapted to the higher average electron beam current. In terms of beam diagnostics, the electron beam current ($3.5A$, $1.5\mu s$) delivered by the injector is a source of trouble. The use of classic OTR or Cherenkov screens to monitor the beam profiles becomes problematic due to the energy deposited inside the screens which is high enough to destroy them [39] if the beam size is kept small as required by the beam transport optimization. For that reason, a non-invasive diagnostic such as a laser wire scanner would be a good solution in measuring the beam profiles. Table 6 shows a summary of the main characteristics of the CTF 3 beam corresponding to the prelinimary and nominal phases.

Parameters	**CTF III preliminary**	**CTF III nominal**
Beam energy (MeV)	*350*	*150*
Bunch charge (nC)	*0.1*	*2.33*
Number of electrons per bunch	$6.25 \cdot 10^8$	$1.45 \cdot 10^{10}$
Bunch length (ps) FWHM	*10*	*10*
Bunch spacing (cm)	*10*	*20*
Number of bunches	*20*	*2310*
RMS Beam Size $\sigma_y(\mu m)$	*150*	*150*
Normalised RMS emittance $(\pi.mm.mrad)$	*50*	*100*
Energy spread (%)	*5*	*10*
Desired waist size σ_w (μm)	*50*	*50*
Repetition rate (Hz)	$5 - 50$	$5 - 50$

Table 6: Characteristics of the electron beam available on CTF 3

For CTF 3 nominal phase, two different laser sources can be foreseen. The first one would use the Nd:YAG $(5 - 10ns, 100Hz)$ laser from the LEP polarimeter which can deliver $100mJ$ at $532nm$ and $200mJ$ at $1060nm$. The other possibility would be to use the CTF 2 laser since this experiment will be stopped by the end of 2002. A $10ps$ laser pulse could be provided with a corresponding energy of $5mJ$ at $523nm$ or $2.5mJ$ at $1047nm$.

Preliminary calculations have been done for both schemes and are summarized in table 7 and 8. Calculations using equation 2.8 have been done for a $50MeV$ electron beam energy and for a $50\mu m$ laser transverse size. The detection solid angle is defined by a half angle of $10mrad$. The results corresponding to the CTF3 preliminary phase $(50MeV)$ have been indicated only in table 7 since the CTF 2 drive laser should not be available before 2003.

Parameters	λ_0= **1.064μm**	λ_0= **532nm**
Laser energy (mJ)	*200*	*100*
Laser pulse duration (ns)	*5*	*5*
Laser power (MW)	*16*	*8*
RMS Beam Size $\sigma_y(\mu m)$	*50*	*50*
Maximum X-rays energy (keV)	*23*	*46*
Number of emitted photons / 15 bunches (N_{sc})	*nominal* *prelim* *$2.3 \cdot 10^4$* *990*	*nominal* *prelim* *4100* *250*

Table 7: Thomson scattered light produced on CTF 3 using the LEP polarimeter laser.

Parameters	λ_0= **1.047μm**	λ_0= **523nm**
Laser energy (mJ)	*5*	*2.5*
Laser pulse duration (ps)	*10*	*10*
Laser power (MW)	*200*	*100*
RMS Beam Size $\sigma_y(\mu m)$	*50*	*50*
Maximum X-rays energy (keV)	*23*	*46*
Number of emitted photons per bunch (N_{sc})	*$1.3 \cdot 10^4$*	*3300*

Table 8: Thomson scattered light produced on CTF 3 using the CTF 2 drive laser

The number of photons is higher using the IR light. With a $5ns$ pulse duration, the Nd:YAG laser would provide an integrating measurement over 15 consecutive electron bunches. In the calculation, the electron characteristics (energy, position, radius) are supposed to be the same for all the bunches. By comparing the results given in table 7 and 8, no significant difference can be seen. The rate of events and the X-rays energy are quite similar so that the detection conditions should be equivalent for both cases. A major difference comes from the fact that using the CTF 2 drive laser, with $10ps$ pulse duration, a bunch to bunch analysis could be performed. On the other hand, the

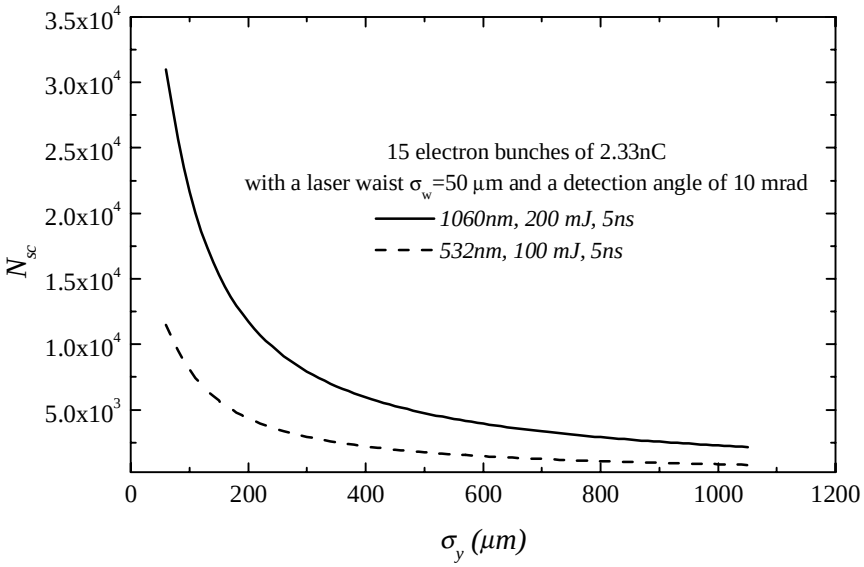

Figure 4-1: Evolution of the number of scattered photons as a function of the electron RMS transverse size

electron-laser beams synchronization should be simpler in the case of the Nd:YAG laser, since one only has to synchronize a $5ns$ laser with a $1.4\mu s$ electron beam.

On figure 4-1, the evolution of the number of events is plotted as a function of the electron beam size. Considering the IR light, the number of events becomes quite low (below 5000 photons) when the electron beam size grows above $500\mu m$. The green light can only be used for very small electron beam sizes. At the end of the combiner ring, the situation will be different since the electron current will be multiplied by a factor of 10, providing, at the entrance of the 35 GHz power extraction sections, a $150MeV$, $35A$ electron beam over $140ns$. Compared to the data indicated here, the number of X-rays scattered out in that condition will be a factor of 10 higher.

During the nominal phase, the maximum electron beam energy at the end of the linac would be $150MeV$. On figure 4-2 the maximum energy of the scattered photons

is plotted as a function of the electron beam energy. If using the infrared light, photons with energies as high as $300keV$ must be detected. The use of the Medipix detector (which should be tested on CTF 2) is limited to the detection of X-rays below $100keV$. This means that for CTF 3, depending on the location of the monitor (and thus electron energy), different kinds of X-ray detectors need to be developed.

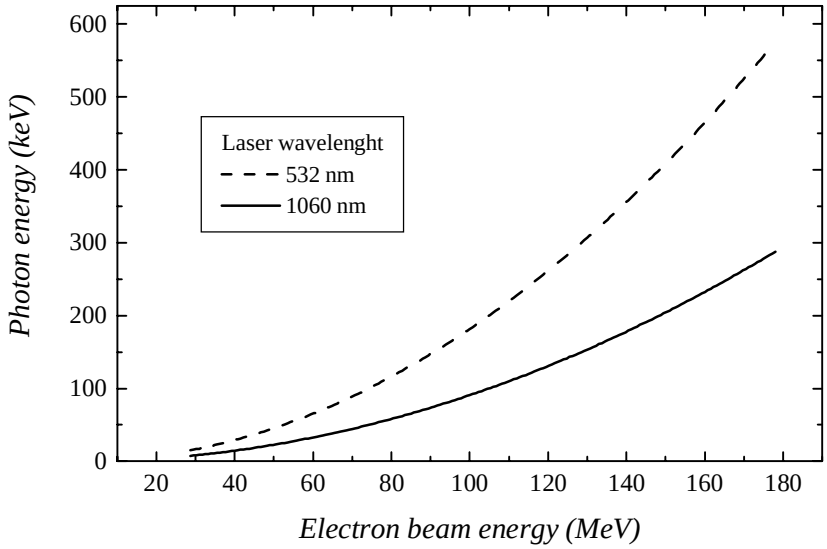

Figure 4-2: Evolution of the maximum energy of the scattered photons as a function of the electron beam energy using equation 2.8.

Chapter 5

Requirements for the CLIC project

For the CLIC project, laser wire scanners would be useful tools for the measurement of transverse beam profiles for both the main beam (high energy $9 - 1500GeV$, low current and very small dimension) and the drive beam (low energy $50 - 1000MeV$, high current). In these extreme two cases, the scattering process is quite different since the energies of the electrons are very different. The case of the CLIC drive beam is similar to the CTF3 beam characteristics and has already been discussed in the previous chapter. Some extrapolations of the laser wire scanner properties are presented in the following section, especially about the behaviour at high energy of the Compton cross section and the corresponding characteristics of the scattered photons and degraded electrons.

5.1 Evolution of the cross section at high energy

The evolution of the Compton cross section is described by the Klein and Nishina equation (equation 1.4), assuming that one replaces the initial factor ξ_0 by $\xi = \frac{\gamma_0 h\nu \quad _0(1-\beta_0 \cos(\psi))}{m_e c^2}$. Figure 5-1 shows the decrease of the Compton cross section as the beam energy increases.

Using a $266nm$ laser and a collision angle of 90 degree, the Compton cross section starts decreasing for an electron beam energies above $1GeV$. For a $50GeV$ electron beam the cross section is reduced by a factor 2. Even if this is not a dramatic effect, it could

be a limitation of the diagnostic capabilities for very high energy beams.

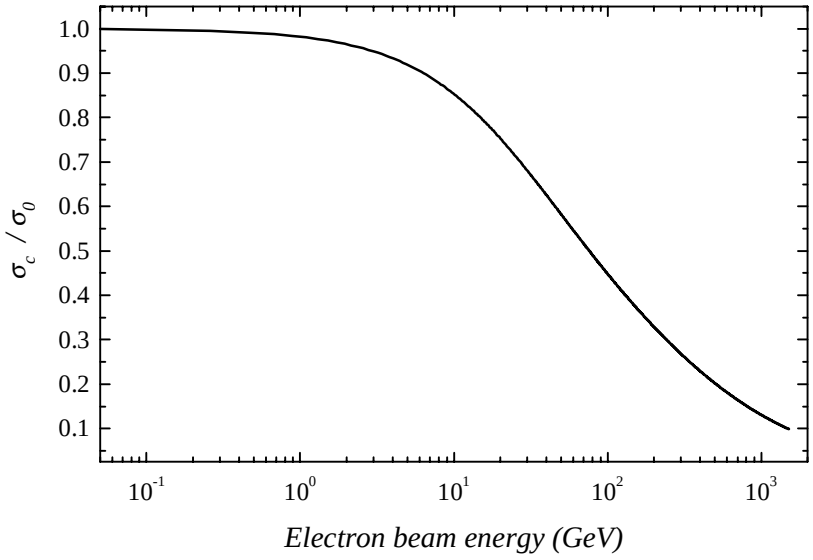

Figure 5-1: Evolution of the scattering cross section as a function of the initial electron beam energy

Moreover the creation of electron-positron pairs is no longer negligible since $\xi \simeq 0.511 MeV$, and the corresponding cross section increases with the electron beam energy [4]. At $1.5 TeV$, the cross section of $e^- - e^+$ pair creation is 20 times smaller than the Compton scattering cross section and these parasitic events would decrease the signal to noise of our detection system.

5.2 Properties of the scattered photons

All along the CLIC main linac (from $9 GeV$ to $1.5 TeV$), beam profile and emittance measurements are required. The energy of the scattered photons depends on the electron beam energy as indicated by the equation 2.3. The γ-ray energy is proportional to $2\gamma_0^2$.

The evolution of the maximum scattered photons energy is plotted on figure 5-2 as a function of the electron beam energy. At very high energy, the initial electron energy is mostly converted into the emission of a high energy γ-ray. During the collision of a $266nm$ wavelength photon with respectively a $500GeV$ and a $1.5TeV$ electron, the energy of the scattered photons can be as high as $473GeV$ and $1.473TeV$.

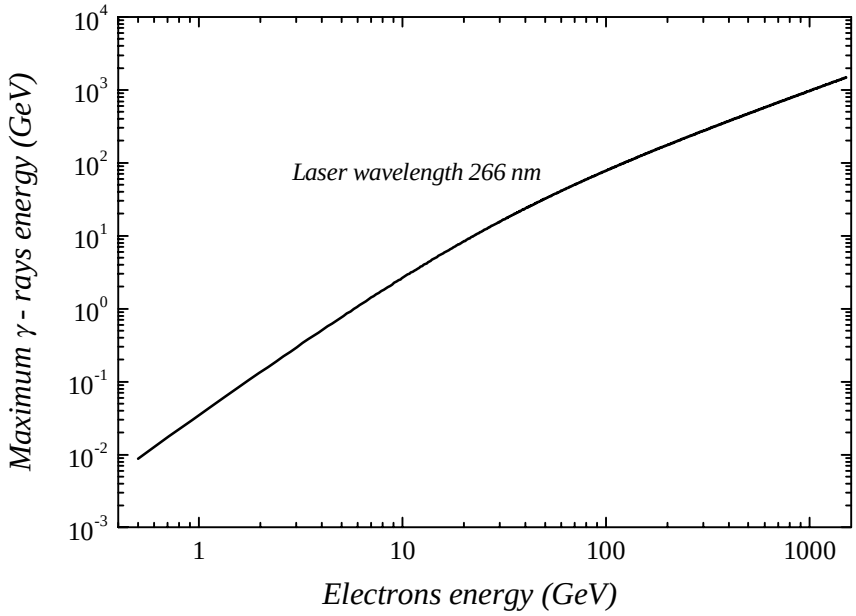

Figure 5-2: Maximum energy of the scattered photons as a function of the incident electrons energy. A 532nm wavelength laser is considered in this case.

Using equation 1.9, the energy spectrum of the scattered photons is calculated for three different laser wavelengths and three electron beam energies, $10GeV$, $500GeV$ and $1.5TeV$. The results are displayed on figure 5-3. Each spectrum has a peak corresponding to the scattered photons of highest energy. The spectrum, which remains rather broad for electron beams of moderate energy, gets sharply peaked around the γ-rays of highest energy for very high energy beams.

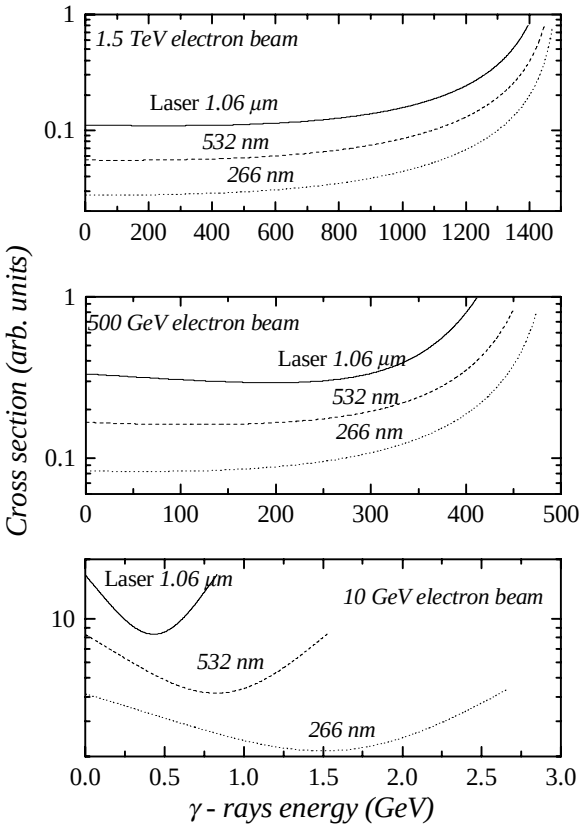

Figure 5-3: Cross section as a function of the γ-ray photons energy. Calculations were done using a 1.06 μm, 532nm and 266nm wavelength laser. (a) In the case of a 1.5TeV electron beam, (b) 500GeV electron beam and (c) 10GeV electron beam.

In a linear collider, the problem of detection is of prime importance. Most of the scattered photon flux is contained in a solid angle of half angle α_c, defined by equation 1.8. On figure 5-4, the evolution of the critical angle α_c is plotted as a function of the electron energy. This calculation is done assuming a 90 degree collision with a 266nm wavelength laser. For a 20MeV electron beam, α_c is about 20$mrad$ and for a 700GeV electron beam, α_c is only of the order of the μrad.

On a linear accelerator, the measurement of the scattered γ-rays will require the

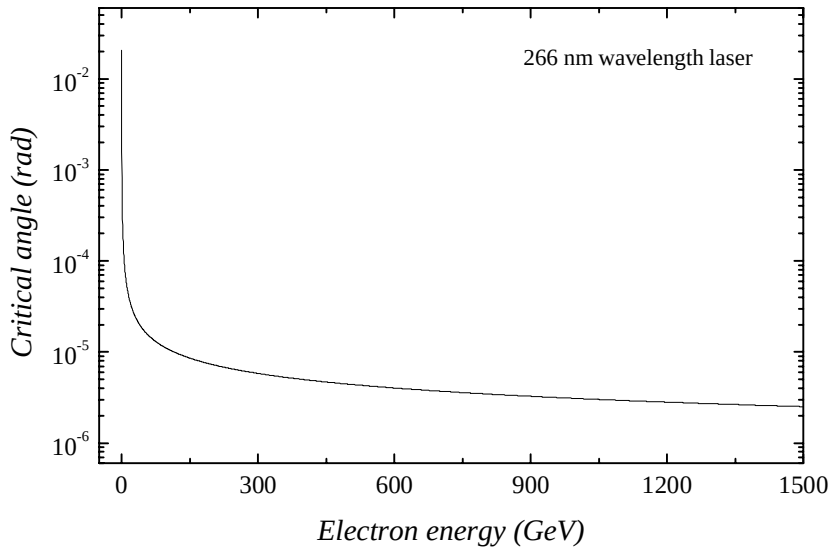

Figure 5-4: Evolution of the critical angle, in which most of the scattered X-rays are contained, as a function of the electron beam energy.

detector to be inserted into the beam line and deviate the electrons. This scheme can be foreseen for electrons of low energy, but it becomes impossible for very high energy. For that reason, the detection of the degraded electrons turns out to be an other interesting possibility. A carefull study of the beam dynamics will be necessary to check where the degraded electrons are lost in order to carefully design and place our detectors.

5.3 Properties of the degraded electrons

The properties of the degraded electrons have been defined previously by equations 1.10 and 1.11. Along the CLIC main linac, the beam energy increases from $9GeV$ to its final value of $1.5TeV$. As said in the previous paragraph, the detection system of a laser wire scanner should be based on the measurement of the degraded electrons. One possibility could be to include in the beam line, just after the interaction zone, a magnetic device

(such as a chicane) in order to separate the degraded electrons from the rest of the electrons. With a lower energy the degraded electrons are strongly deviated and sent onto an appropriate detector. The other electrons are just slightly deviated, and they can pursued their initial trajectory, as shown on figure 5-5.

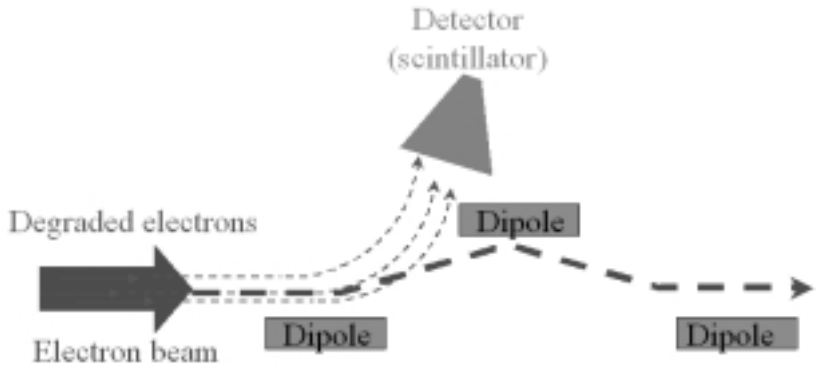

Figure 5-5: Scheme of the detection of the degraded electrons

The efficiency of the detection is based on its capability to separate the degraded electrons from the rest of the beam. The design of such a device must then be adapted to the energy of the degraded electrons. When the electron beam energy is not very high (tens of GeV), the recoil of the particules in the collision is still quite low. On figure 5-6, both the energy spectrum and the scattering angle of the degraded electrons are shown assuming a collision between a $266nm$ wavelength laser and a $10GeV$ electron beam (equivalent to the conditions at the entrance of the CLIC main linac). The maximum energy loss corresponds to 25% of its initial value and is associated to a $0.05\mu rad$ scattering angle. The scattering angle distribution is centered in the μrad range. Anyway, even if simulations are needed to investigate the corresponding beam transport, the energy difference between the degraded electrons and the rest of the beam is so small that the efficiency of the chicane would be very poor. For this reason, other diagnostics, such as classical wire scanners or OTR screens would be better suited to measure the beam profiles at the entrance of the main linac.

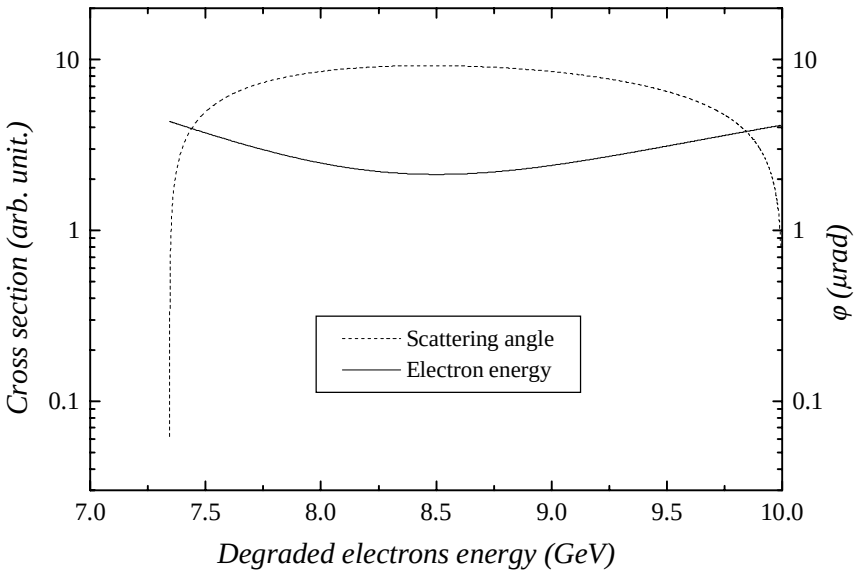

Figure 5-6: Energy spectrum and scattering angle of the degraded electrons produced by Compton scattering between a $266nm$ wavelength laser and a $10GeV$ electrons beam.

For energies above 100 GeV, the electron recoil becomes very strong. On figure 5-7 (a), the behaviour of the scattering angle of the degraded electrons is shown. The shape of the distribution does not change when the electron beam energy increases. The energy spectrum of the degraded electrons is shown on figure 5-7 (b) considering a $266nm$ wavelength laser and $100GeV$, $500GeV$, $1TeV$ and $1.5TeV$ electrons respectively. The shape of the spectrum is getting sharper and sharper when increasing the electron energy, but the minimum energy of the degraded electrons, E_{min}, does not change significantly. It varies from $21.6GeV$ for a $100GeV$ electron beam to $27.2GeV$ for a $1.5TeV$ beam. Above a given energy, the design of the chicane and the choice of the detector could be the same and should be adapted to the measurement of $27GeV$ electrons. This is a very nice feature in terms of reducing the cost and the amount of work needed to develop the diagnostic.

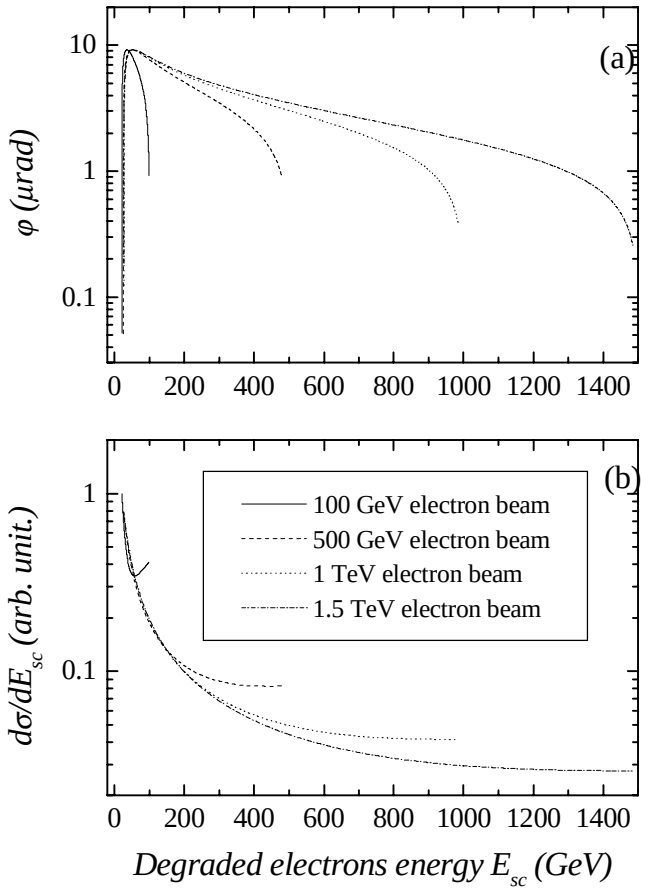

Figure 5-7: Scattering angle (a) and energy spectrum (b) of the degraded electrons produced by Compton scattering using a $266nm$ wavelength laser. The different curves correspond to electron beam with initial energies of $100GeV$, $500GeV$, $1TeV$, $1.5TeV$. Calculations were done using equations 1.11 and 1.10.

Chapter 6

Conclusions

Several laser wire scanners have been already developed during the past five years on electron beams of low energy ($50MeV$) [20], intermediate energy ($4GeV$) [23] and high energy [22] ($50GeV$). In all cases, the results indicate that the diagnostic works well. It is important to notice that a major difficulty arises from the X-ray or γ-ray background noise. This makes the diagnostic very sensitive to beam losses.

For CLIC, laser wire scanners would be useful to measure the beam profiles for both the main beam (high energy 9-1500 TeV, low current and very small dimension) and the drive beam (low energy 50-1000 MeV, high current). In these two cases, the scaling laws of the scattering process are different since the energy range of the electron is also very different (From Thomson to Compton regime). A general formulation has been proposed to calculate the properties of the scattered photons. In a LWS the collision angle between the electron and the laser beams is set to 90 degree. Due to a double doppler shift, the energy of the scattered photons is multiplied by a factor $2\gamma^2{}_0$, producing X-ray or γ-ray beams. Moreover, most of the scattered photons are contained in a small solid angle centered on the initial direction of propagation of the electrons. The main difference between the Thomson (low energy) and the Compton (high energy) regimes is that in the Compton regime the electrons recoil is not negligible, since the electrons will loose an important part of their initial energy in the collision. At low energy, the detection

system must be based on the measurement of the scattered X-rays, where for high energy electrons, the measurement of the degraded electrons becomes a better way of detection. Unfortunately, for intermediate electron energies of the order of $10GeV$, the detection of both the scattered photons and the degraded electrons is difficult. That's why the use of other diagnostics such as OTR screens or classic wire scanners should be preferred in monitoring the beam profiles at this energy. For the CLIC main beam at very high energies ($> 100GeV$), beam dynamic simulations need to be done in order to design an appropriate system for the detection of these degraded electrons.

Some calculations to scale the laser wire scanner parameters on CTF2 and CTF3 have been presented. For both cases, the possibility of building such an experiment was found without having to purchase a high power laser (which is quite expensive in the order of 300 kCHF). The CTF 2 photocathode laser and the LEP polarimeter laser could be used for that purpose. The LWS would be well adapted to the measurement of small size electron beams. Calculations have shown that for transverse beam sizes above $1mm$, the diagnostic would probably not be very efficient since the number of scattered photons depends strongly on the electron beam density. On CTF 2, the aim will be to define and to quantify precisely the performance and the reliability of such a diagnostic and to develop appropriate X-ray detectors. A first test of X-ray background measurements is already underway. For CTF 3 and afterwards for the CLIC drive beam, the LWS could become a useful monitor to replace the classic Transition Cherenkov Monitor which can not be used with the full electron current.

For CTF2 and CTF3, the focusing system of a laser wire scanner does not represent a major challenge. It could be implemented using classic laser sources and optics. To go down to very small laser beam spot size, one has to use short wavelength lasers. Using the existing technology, a $266nm$ wavelenght laser is a good compromise providing sufficient power and good reliability. Even if shorter wavelength laser are currently studied, for example for lithographics applications, there is no existing system available at the present

time. In the previous experiment at SLAC, the minimum spot size obtained was in the order of twice the laser wavelength [21]. With green light ($532nm$) or UV light ($266nm$), one should be able to achieve a $1\mu m$ laser spot size over a total distance of $13\mu m$ and $25\mu m$ respectively, so that the ratio between the transverse electron dimensions, σ_y/σ_x should not be larger than 25. For the CLIC main linac, the FODO lattice should be modified in order to obtain a location where the beam aspect ratio is compatible with the laser focusing capabilities. An other possibility for measuring smaller electron beam sizes is the laser interference pattern proposed by Shintake [30] and already tested at SLAC at the Final Focus Test Beam [31]. This device, which is based on Compton scattering too, is more complicated in terms of optics adjustements. Electron beam sizes of $40nm$ have been measured with this method.

Bibliography

[1] J.J. Thomson, *Notes on Recent Researches in Electricity and Magnetism, Oxford, U.K., clarendon Press, (1893) .*

[2] A.H. Compton, *Phys . Rev. 22, (1923), 409.*

[3] O. Klein and Y. Nishina, *Z . Phys. 52, (1929), 853*

[4] Bruno Rossi, "*High Energy Particles", Prentice hall Incorporation, (19 52).*

[5] F.R.Arutymian and V.A. Tumanian, *Phys . Rev. 4, (1963), 176.*

[6] R.H. Milburn., *Phys . Rev. Lett. 10, (1963), 75.*

[7] G. Fiocco and E. Thompson, *Phys . Rev. Lett. 10, (1963), 89.*

[8] S.C. Chen and T.C. Marshall, *Phys . Rev. Lett. 52, (1984), 425.*

[9] C.K. Sinclair et al, *IEEE Trans . on Nucl. Sc. 16, (1969), 1065.*

[10] J.R. Sauer et al, *IEEE Trans . on Nucl. Sc. 16, (1969), 1069.*

[11] L.F. Giodarno et al, *Nuovo Cimento 59, (1980), 247.*

[12] I.F. Ginzburg et al, *Sov. J. Nucl. Phys. 38, 2, (1983), 222.*

[13] T. Yamazaki et al, *IEEE Trans . on Nucl. Sc. 32, (1985), 3406.*

[14] P. Maine et al, *IEEE J. Quantum Electronic 24, (1988), 398.*
C. Le Blanc et al, *Optics Letters 18, (1993), 140 .*

[15] P. Sprangle et al, *Journal of Appl. Phys. 72, (1992), 5032.*
E. Esarey et al, *Phys. Rev. E 48, (1993), 3003.*

[16] H. Burkhardt et al, *CERN 99-10, (1999).*

[17] D. Fargion et al, *Z. Phys. C 74, (1997), 571.*

[18] K.J. Kim, *NIM A 341, (1994), 351.*

[19] T. Shintake, *NIM A 311, (1992), 453.*

[20] W.P. Leemans et al, *Phys. Rev. Lett. 77, (1996), 4182.*

[21] M.C. Ross et al, *Proceeding of the LINAC conference, Geneva, (1996), 308.*

[22] R. Alley et al, *NIM A 379, (1996), 363.*

[23] H. Sakai et al, *Phys. Rev. Spec. Topics- Accelerators and Beams, 4, (2001), 022801.*
H. Sakai et al, *NIM A 455, (2000), 113.*

[24] S.K. Ride et al, *Phys. Rev. E 52, (1995), 5425.*

[25] D. Meyerhofer, *IEEE Journal of Quantum Electronics. vol 33, (1997), 1935.*

[26] C. Bula et al, *Phys. Rev. Lett. 76, (1996), 3116.*

[27] C.I. Moore et al, *Phys. Rev. Lett. 74, (1995), 2439.*

[28] A.E. Siegman, "*Lasers", Oxford university press, (1986), 668-669.*

[29] ZEMAX optical sotfware: see http://www.focus-software.com/

[30] T. Shintake et al, *NIM A 311, (1992), 351.*

[31] V. Balakin et al, *Phys. Rev. Lett. 74, (1995) 2479.*
T. Shintake et al, *Proceeding of the 1995 PAC Conference, Dallas.*

[32] K.J. Kim, *Physics of Particles Accelerators, eds M. Month and M. Diene, AIP Conf. Proc. 184 (AIP New York 1989), Vol 1, 565.*

[33] F.V. Hartemann et al, *Phys. Rev. E 64, (2001), 016501.*

[34] The CLIC Study Team, *"CTF2 design report", CERN/PS 96-14, (1996).*

[35] W. Schnell, *"A Two Stage RF Linear Collider Using a Superconducting Drive Linac", CLIC note 13, CERN LEP-RF/86-06, (1986).*
W. Schnell, *"The CLIC Study of an Electron-Positron Collider", CERN SP/92-51, CLIC note 184, (1992).*

[36] M. Dehler, *"Modeling of a 30 GHz Waveguide Loaded Detuned Structure for CLIC", CLIC note 358 (1998)*
M. Dehler, R. M. Jones, N. M. Kroll, I. Wilson, W. Wuensch, *"Design of a 30 GHz Damped Detuned Accelerating Structure", CERN PS/97-26 (LP) 1997 ; Proceeding of the 1997 PAC Conference, Vancouver, (1998), 518.*
H.H. Braun, S. Doebert, L. Groening, I. Wilson, W. Wuensch, F. Zhou, "High-Power testing of 30GHz Accelerating Structures at the CLIC Test Facility (CTF II), CERN/PS 2001-009 (AE).

[37] H Braun et al, *CERN/PS 2000-034 (2000).*

[38] H Braun et al, *CLIC note 441, CERN/PS 2000-030 (2000).*
H Braun et al, *CERN/PS 2000-034 (2000).*
H Braun et al, *CERN/PS 2000-056 (2000).*

[39] E. Bravin, *CTF3 note 019, (2001).*

[40] The CLIC Study Team, *"Proposals For Future CLIC Studies and a New CLIC Test Facility (CTF3)", CLIC note 402 (1999).*

[41] M. Chmeissani and B. Mikulec, *NIM A 460, (2001), 81.*
B. Mikulec et al, *NIM A 458, (2001), 352.*